Study of the Velocity and Strain Fields in the Flow Through Prosthetic Heart Valves

A. López-Zazueta

R. Ledesma-Alonso

J. E. V. Guzman

R. Zenit[1]

e-mail: zenit@servidor.unam.mx

Instituto de Investigaciones en Materiales,
Universidad Nacional Autónoma de México,
Coyoacan 04510,
Mexico D.F., Mexico

A comparative experimental study of the velocity field and the strain field produced down-stream of biological and mechanical artificial valves is presented. In order to determine the spatial and temporal distributions of these fields, a phase-locked stereoscopic particle image velocimetry (or 3D-PIV) technique was implemented. Emphasis was placed on the identification of the fundamental differences between the extensional and the shear components of the strain tensor. The analysis of the characteristic flows reveal that the strains in every direction may reach high values at different times during the cardiac cycle. It was found that elevated strain levels persist throughout the cardiac cycle as a result of all these contributions. Finally, it is suggested that the frequency with which the strain variations occur at particular instants and locations could be associated to the cumulative damage process of the blood constituents and should be taken into account in the overall assessment of existing valve types, as well as in future design efforts. [DOI: 10.1115/1.4005475]

Keywords: Cardiac valve prosthesis, Transvalvular flow, Strains, Blood damaging potential

1 Introduction

Heart valves that fail to perform their physiological function correctly can be replaced either by mechanical or biological prosthetic valves. Despite the abundant variety of models and their continuous improvement over the years, current designs are far from perfection and unresolved questions concerning transvalvular flows persist [1].

In terms of hemodynamic performance, biological valves are generally considered to be superior to their mechanical counterparts because their thrombogenic potentials are similar to the ones observed in native human valves [1]. Nevertheless, owing to calcification processes, tissue overgrowth and leaflet wear, their durability is limited to about 15 years. Mechanical valves, on the other hand, last much longer but possess design-related problems such as highly irregular flows, regurgitation, leakages, and stagnated fluid regions, which cause severe blood cell damage and thrombosis.

Many studies indicate that the elevated shear and turbulent stresses commonly produced in the transvalvular and downstream flow regions could induce membrane disintegration (lysis), multiple cell-to-cell collisions, coagulation, unfolding and activation of platelets and blood factors, as well as aggregate formations [2–5]. In addition, the exposure time to these conditions has been identified as a critical factor in the damaging and activation processes [6,7].

The effects produced on platelets by actual flows in artificial valves were studied by Bluestein et al. [8] who conducted some in vitro experiments with the Björk-Shiley valve. In a complementary study the fundamental relation between turbulent stresses and platelet activation in Carbomedic and Björk-Shiley valves was surveyed by Yin et al. [9]. Interestingly, however, neither of these investigations involved experimental evaluations of the particular flows produced in those valves.

Several current experimental investigations are aimed at producing detailed descriptions of the flow field across valves by recursing to advanced measuring methods such as the Laser Doppler Anemometry [10,11], or optically based methods that allow observations with enhanced resolutions. For instance, variations of the particle image velocimetry (or PIV) technique have been successfully exploited in the study of jets [12], regurgitations [13] and high time-resolution velocity profiles [14] in common mechanical valves. Also, the Reynolds stresses produced by porcine bioprosthetic valves have been mapped under steady and pulsatile flow conditions [15,16].

The potential of the 3D-PIV techniques for reconstructing the spatial structure of the flow field around the valves was illustrated by Marassi et al. [17] and by Amatya et al. [18]. In the first case a mechanical bileaflet valve and a pericardium valve were tested in the presence of pulsatile flows. In the second case a St. Jude bileaflet prosthesis was tested in a steady flow and an experimental bileaflet trial model was analyzed in a pulsatile flow. It must be emphasized that, although the authors provided the spatial distributions of the flow fields, the strains were not evaluated and further testing was recommended.

On this account, an evident need to further investigate the spatial and temporal distributions of the velocities and the strains produced downstream of the artificial valves is identified. The question about the strains in the transvalvular flow region is of a fundamental character. Schnider et al. [7] discovered that the von Willebrand factor (one of the key elements involved in the coagulation process) becomes activated beyond a certain level of the velocity gradient in a simple shear flow. It must be noted that the stress levels corresponding to these shears are much lower than those reported for the activation of platelets or for damaging red blood cells [7]. Furthermore, in the general case of a complex flow field, the velocities may change substantially in all directions; hence, although the threshold level for the activation of the von Willebrand factor has been identified for the case of simple shear flow, it is imperative to assess the magnitude of the other components of the velocity gradient tensor.

It can be argued that certain types of deformations can cause the von Willebrand factor to become active at even lower

[1]Corresponding author.

Contributed by the Bioengineering Division of ASME for publication in the JOURNAL OF BIOMECHANICAL ENGINEERING. Manuscript received May 24, 2011; final manuscript received November 15, 2011; published online December 21, 2011. Assoc. Editor: Fumihiko Kajiya.

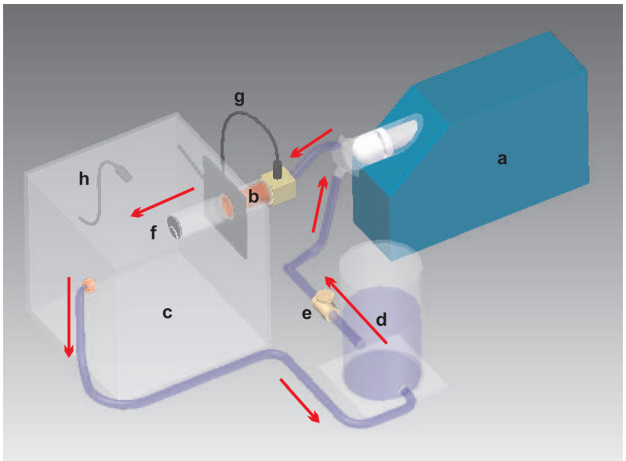

Fig. 1 Components of the flow circuit: (*a*) pulsatile pump, (*b*) laminarization section, (*c*) test section, (*d*) compliance chamber, (*e*) needle valve, (*f*) valve, (*g*) upstream pressure transducer, (*h*) downstream pressure transducer.

threshold values if the extensional components are comparable to the shear components. It has been shown, for instance, that for the case of droplets the deformation is much larger if the flow is extensional rather than shearing [19]. In view of this results the same effect could be expected to be relevant in the case of proteins and other blood constituents.

Therefore, understanding the relative importance of the components of the strain tensor becomes crucial. It may finally be noted that accurate measurements of the velocities, velocity gradients and stresses are required as inputs by the semiempirical models used to evaluate the blood damaging potential [4,20–22].

In this context the present work provides a detailed comparative view of the flow structures produced by biological and mechanical artificial valves and, thereby, complement previous findings. Two of the most common mechanical models (St. Jude Medical and the Björk-Shiley) and two bovine pericardium models (INC-Mexico) were tested. The focus of the investigation was placed on the phase-averaged strain distributions and their magnitudes downstream of the valves. The primary objective was to establish the relative importance of the extensional and shear components of the strain tensor. A phase-locked stereoscopic particle image velocimetry (3D-PIV) technique was implemented to determine the rapid variation of the velocity fields, and to identify the stagnation and agitated flow regions, in order to link them to the cumulative straining history.

2 Experimental Program

2.1 Test Apparatus. Experiments were performed using a flow circuit based on the Windkessel model which emulates the basic dynamic characteristics of the human circulatory system [23,24] (Fig. 1).

A pulsatile pump (Harvard Apparatus 1200 series) was connected, through a check-valve, to a laminarization chamber at the inlet of the valve support. The cylindrical support for the valves was made of a transparent (acrylic) tube with an internal diameter of 50 mm and a length of 300 mm. The prostheses were placed at one end of the support facing toward a damping chamber which consisted of a transparent cube with a length of 0.35 m. The geometrical characteristics of the prostheses used here are summarized in Table 1. In order to reproduce the elastic response of major arteries to the pulsatile flow, a compliance tank was installed at the outlet of the test section. The equilibrium pressure inside the compliance tank was set to 1 atm for the no-flow condition. The effects of the capillary vessels were simulated by a needle valve connected between the compliance tank and the pump.

Table 2 Experimental flow parameters: V_s is the volume stroke, f is the heart rate (frequency). The systolic fraction indicates the duration of the systole as a percentage of the total cardiac cycle.

Case	V_s (cm^3)	f (s^{-1})	Systolic fraction (%)
*A*1 (Bioprosthesis 1)	45	0.4	0.35
*A*2 (Bioprosthesis 1)	50	0.5	0.35
*A*3 (Bioprosthesis 2)	90	1.0	0.35
B (Bileaflet)	45	0.4	0.35
C (Monoleaflet)	85	1.2	0.35

Pressure transducers were installed upstream of the test section and on the reservoir (at the same height) to determine the pressure drops across the valves. It is remarked that the "laminarization" chamber located upstream of the test section produced a regular flow field (as indicated by PIV measurements). Therefore, the values registered by the corresponding transducer were considered to be reliable reference pressures for the calculation of the overall pressure drop. The corresponding readings were acquired with a National Instruments PCI-6010 data acquisition system and synchronized with the velocimetry measurements.

Water was used as the working fluid because the PIV technique requires an optically transparent medium. This choice was further justified from the dynamical point of view, since the viscosity of the blood flowing through the heart and large vessels is predominantly determined by the blood plasma, which behaves as a Newtonian fluid. In contrast, non-Newtonian (shear-thining) effects would be relevant in small vessels, whence the deformability and concentration of the blood cells contribute to modify the viscosity [23,25,26]. The parameters corresponding to the five different flow conditions under consideration are summarized in Table 2. These values are reported in the calibration certificate of the manufacturer (Harvard Apparatus) and an independent verification was carried out in the laboratory to verify that the mean flow rate was indeed given by $\langle G \rangle = V_s \cdot f$.

It is important to emphasize that the elasticity of the vascular walls in the arterial tree and the presence of sinus cavities (downstream of the valve) were not modeled in our experiment, but have a definite influence on the overall dynamical development of the blood flow downstream of a valve (e.g., Ref. [23]). Results concerning the complex evolution of the flow within these regions

Table 1 Tested prosthetic heart valves and their geometric characteristics: d_i is the internal diameter, d_o is the maximum opening diameter and θ is the maximum leaflet opening angle. The prostheses were provided by the Instituto Nacional de Cardiología of Mexico (INC).

Type	Design	d_i (cm)	d_o (cm)	θ (deg)
Stented bioprosthesis 1 (A1, A2)	INC-Mexico, Bovine	3.0	1.4	60–90
Stented bioprosthesis 2 (A3)	INC-Mexico, Bovine	2.5	1.8	60–90
Bileaflet (B)	St. Jude Medical, Regent	2.4	2.1	85
Tilting-disc (monoleaflet) (C)	Björk-Shiley, convexo-concave	1.8	1.7	60–70

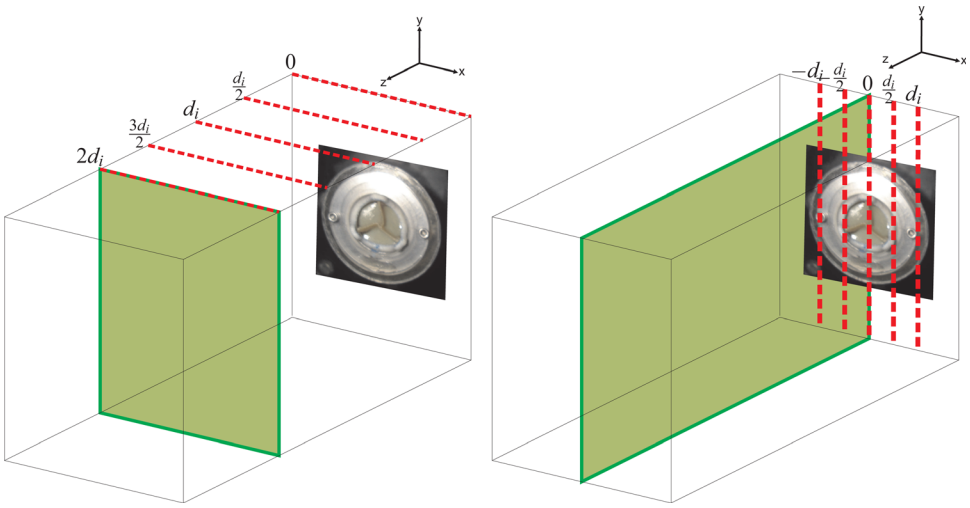

Fig. 2 The positions of the measurement planes are indicated by red dotted lines. (left) For cases *A*1, *A*2, and *B*, the planes are perpendicular with respect to the direction of the flow. (right) For cases *A*3 and *C* the planes are parallel with respect to the direction of the flow. The separation between planes is given by $d_i/2$, with d_i taken from Table 1 for each valve.

and its relation with valve dynamics and blood damage have been reported by Dasi et al. [33].

2.2 Measurement Techniques. A stereoscopic particle image velocimetry (3D-PIV) technique was implemented to quantify the flow field downstream of the valves. The fluid was seeded with silver coated glass spheres of 50 μm to reflect the pulsed light from a 0.5 mm thick laser sheet generated with a 532 nm Nd:YAG Laser. Two Kodak Megaplus ES1.0 CCD cameras, with a 1008×1016 pixel resolution, were placed at angles that varied in the range 20 deg to 90 deg in conformity with the typical stereoscopic arrangement [17,18]. Interrogation areas of 32×32 pixels with a 50% overlap were defined for vector processing and the time between snapshots ranged from 100 μs to 3000 μs, depending on the particular moment of the cycle being analyzed. It must be noted that the spatial resolution of the equipment only allows accurate measurements of the macroscopic flow structures. In this context, the size of the PIV tracer particles has no significant effect on such structures.

The volume of interest was divided by five perpendicular planes, with respect to the direction of the flow, for cases A1, A2 and B, and by five parallel planes for cases A3 and C (as shown in Fig. 2). The separation between planes was $d_i/2$ mm, where d_i corresponds to the valve's internal diameter indicated in Table 1. The operating cycle was evenly divided in 10 time intervals for cases A1, A2 and B, and in 16 for cases A3 and C (10 partitions for the opened position and 6 for the closed position, respectively). A "phase-locking" technique was implemented to produce 250 independent measurements of the mean and the fluctuating velocities for the specified instants along the operating cycle of the valve. In this manner a phase-average of the velocity field, v_i, was obtained with both spatial and temporal resolution. To further improve the visualization of the flow, the velocity field was spatially interpolated considering a spline scheme for which $\Delta x = \Delta y = 1.2$ mm.

The phase-averaged velocities were used to evaluate the velocity gradients

$$\underline{\underline{L}} = \left(\frac{\partial v_i}{\partial x_j}\right) \tag{1}$$

where v_i and x_i represent the velocity and the position oriented along the "ith" direction, respectively. The strain tensor corresponds to the symmetrical part of the velocity gradient and was calculated as

$$\underline{\underline{D}} = \frac{1}{2}\left(\frac{\partial v_i}{\partial x_j} + \frac{\partial v_j}{\partial x_i}\right) \tag{2}$$

The extensional and shear strains of the flow field were determined from Eq. (2) for the prescribed spatial locations and time intervals. Finally, the magnitude of the strain at the point of interest were evaluated considering

$$\left|\underline{\underline{D}}\right| = \sqrt{\frac{1}{2}\sum_{i,j} D_{ij} \cdot D_{ij}} \tag{3}$$

2.3 Measurements Uncertainties. The issue of uncertainty in the measurement of velocity gradients via optical techniques has been addressed by several authors (e.g., Refs. [27,29], among others). Since the calculation of these quantities depends on the spatial derivatives of the measured velocity, their uncertainty must be assessed. Considering the Kline and McClintock's procedure (cf. Ref. [28]), the uncertainty in the measurement of the strain tensor δD_{ij} can be calculated as

$$\frac{\delta D_{ij}}{\langle D_{ij}\rangle} = \left[\left(\frac{\delta U}{\langle U\rangle}\right)^2 + \left(\frac{\delta \lambda}{\langle \lambda\rangle}\right)^2\right]^{1/2} \tag{4}$$

where $\langle D_{ij}\rangle$ is the measured value of the strain tensor. δU, $\delta\lambda$, $\langle U\rangle$, and $\langle\lambda\rangle$, are the uncertainty and mean value of the velocity and length, respectively. This expression considers that the uncertainties of $\langle U\rangle$ and $\langle\lambda\rangle$ are uncorrelated. Considering relative uncertainties of 4% in both velocity and length, a value of $\delta D_{ij}/\langle D_{ij}\rangle \approx 5.6\%$ is expected. However, the measurement of velocity gradients is greatly affected by truncation errors, as discussed by Ref. [29]. The truncation error, T_{ij}, can be calculated from the expression proposed by Ref. [27]

$$T_{ij} = -\frac{1}{6}\frac{\partial^3 u_i}{\partial x_j^3}(\delta x_i)^2 \tag{5}$$

where the repeated indices do not imply summation. This expression considers a four point central difference scheme to obtain the velocity derivatives. In our case we have measured that $(T_{ij})_{\max}/(\langle U\rangle/\langle\lambda_{\max}\rangle) \approx 0.148$, where $\lambda_{\max}$ is the separation distance in between measuring planes. Following the arguments

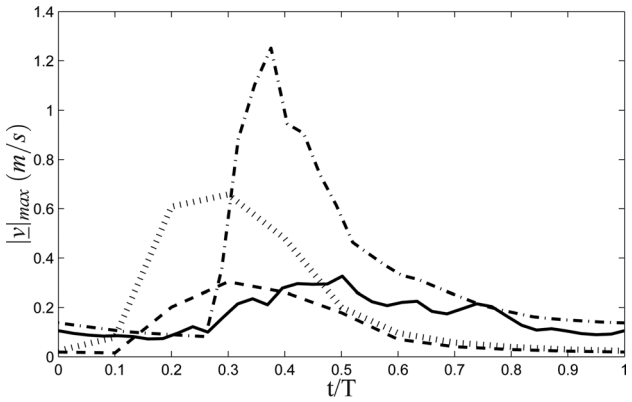

(a)

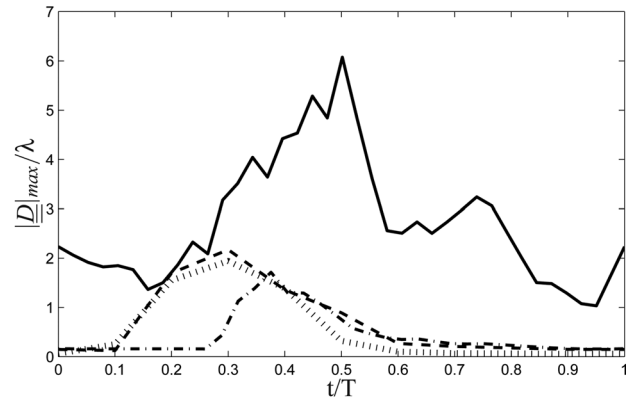

(b)

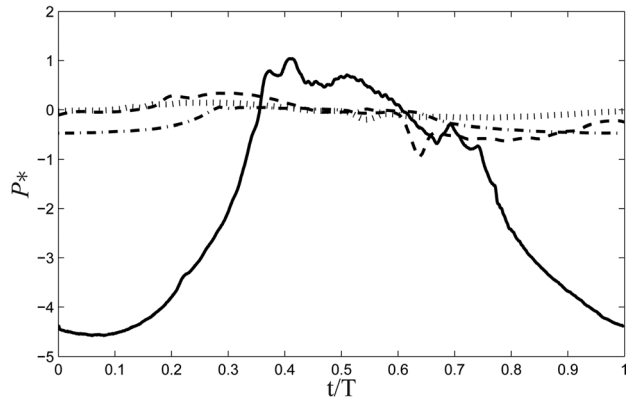

(c)

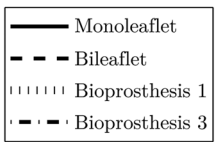

Fig. 3 (*a*) Maximum velocities, (*b*) Maximum normalized strains, (*c*) Maximum normalized pressure drop. All quantities are phase-averaged.

proposed by Özcan et al. [27], we estimate that the uncertainty of the measurement is roughly twice the truncation error; hence, $\delta D_{ij}/\langle D_{ij}\rangle \approx 29\%$. Although the uncertainty is relatively large, the variation observed in the mean trends are larger than the uncertainty level. Therefore, we are confident that the present measurement gives us a correct trend which is important to determine the mechanisms of blood trauma. To reduce the uncertainty, measurements would have to be obtained in more closely spaced planes; the amount of work that this would imply is unsurmountable. We plan to improve the accuracy of measurement in this type of flows by considering, in the future, the use of a true volumetric PIV system such as that used by Amatya et al. [18].

3 Results

3.1 Velocity Fields. The results for the maximum average velocities are presented in Fig. 3(*a*). It can be clearly seen that biological valves produce significantly higher velocities (in the range 0.6 m/s to 1.25 m/s) than their mechanical counterparts (~0.3 m/s) for similar nominal conditions. Although all peak values are attained within the $0.3 \leq t/T \leq 0.5$ interval, the velocity profile of the tilted disk valve is quite irregular as compared to other designs.

The structural details of the average velocity fields for valves A3, B, and C, are shown in Fig. 4. The velocity is normalized in terms of the (absolute) maximum average velocity, $|\underline{v}|_{\max}$; the adopted color convention is: red for the highest value and blue for the lowest. In biological valves (top row) a very distinctive axial jet is formed without secondary circulations near or downstream of the valve during the operation. In contrast, a bileaflet valve induces a richer structural organization of the flow field. During the opening stage two characteristic, high-speed jets are formed at either side of the valve. These side jets merge with the slower central flow at $t/T \approx 0.4$. Toward the end of the closure process, a residual flow proceeds downstream in response to the previously formed eddies. Monoleaflet valves; on the other hand, have nonzero velocity components even if they are closed. These leakages perturb the fluid located directly ahead of the valve until the following cycle initiates. Moreover, the asymmetrical jets produced by this valve type leads to a more complex (coupled) interaction between the resulting eddies. Such observations are in agreement with previous investigations [1,10,11].

3.2 Maximum Strain Fields. A comparison of the maximum strains produced by each valve during the operating cycle is illustrated in Fig. 3(*b*). The values are normalized in terms of a characteristic frequency given by $\lambda = |\underline{v}|_{\max}/d_o$, where d_o is the opening diameter of the valve (see Table 1).

Substantially higher strain values were registered for the monoleaflet design. The other valves had a similar performance with the biological model (case A3) producing the lowest value. The corresponding constant strain surfaces are shown in Fig. 5. Three constant levels of $|\underline{\underline{D}}|/\lambda$ are shown for each valve. Clearly, the biological valve induced a "well behaved" strain field as illustrated by the corresponding sequence of images. It is observed that spatially regular surfaces accompany the central jet during the aperture. Also, a high strain core evolves (concentrically) downstream with its peak value occurring at $t/T \approx 0.38$. Toward the end of the cycle, the low strains observed in the wake of the jet have completely dissipated.

For the case of the bileaflet prosthesis (St. Jude Medical) the highest strain values are reached during the aperture at the cores of the double-jets. With the merging of the jets, a complex bundle of interacting strain regions is observed. Nonetheless, some regularity still remains in the overall structure. At the mid-cycle ($t/T = 0.5$) the structure has evolved, in such a way, that alternating regions of high and low shear stresses may result from the interacting fluid regions (as suggested by the black band between the two red and blue regions). The cycle ends rather quickly as evidenced by the lack of activity near the valve (only the wake can be seen during this stage).

The monoleaflet valve (Björk-Shiley) showed a significantly different behavior. A sharp contrast is noted between strain produced by the monoleaflet and the previous two designs. The complex flow structure strongly suggests the appearance of turbulentlike eddies throughout the cycle. More relevant is the fact that

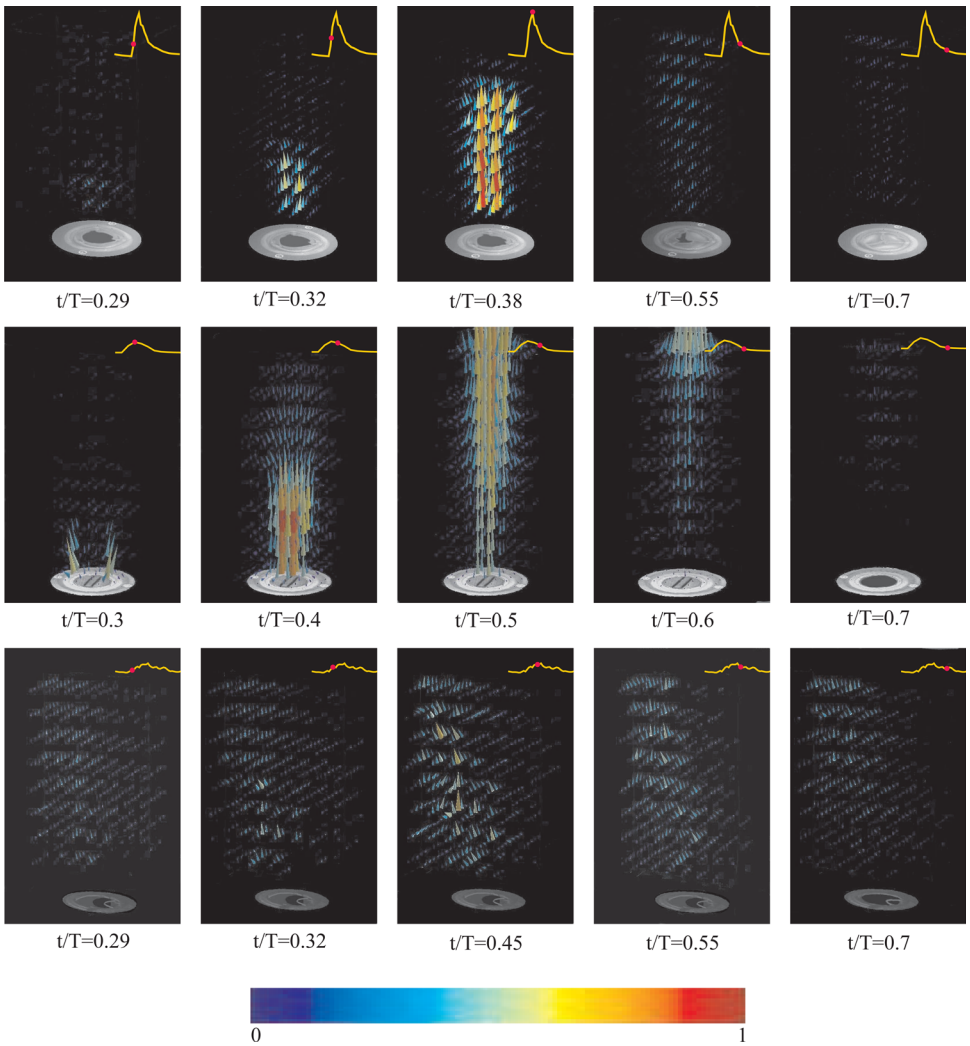

Fig. 4 Velocity fields produced by the selected valves. The first, second and third rows correspond to the biological *A*3, the bileaflet, and the monoleaflet valves types, respectively. The images in any given row represent a time sequence for the valve within one period, *T,* of the operating cycle. The highest normalized velocities are shown in red and the lowest in blue according to the color scale at the bottom. Additionally, an insert at the upper right corner of each image shows the peak velocity, $|\underline{v}|_{\max}$, measured at that particular instant of the cardiac cycle [actual values can be read from Fig. 3(*a*)]. The photo of the valve at the particular flow condition appear at the bottom of each image.

very high shear regions are "exposed" to weakly strained regions (as can be seen at times $t/T \approx 0.45$ and 0.55), and that such mixed regions are widely spread around the valve.

Finally, the pressure losses produced by each valve type are related to the irregular distribution of the transvalvular stresses. Thus, their respective pressure drops were computed with

$$P^* = \frac{P_{\text{downstream}} - P_{\text{upstream}}}{\frac{1}{2}\rho v_{\max}^2} \tag{6}$$

where $P_{\text{downstream}}$ and P_{upstream} represent average values, and $\frac{1}{2}\rho v_{\max}^2$ is the kinetic energy per unit volume of the flow. The corresponding curves are plotted in Fig. 3(*c*). It is noteworthy that the transvalvular pressure drop caused by the monoleaflet valve is much higher than in other cases [Figs. 3(*a*) and 3(*b*)].

3.3 Detailed Description of the Strain Fields. The maximum average strains [Fig. 3(*b*)] and their corresponding magnitudes (Fig. 5) can only provide a limited view of the strains in the flow field. Nevertheless, deeper insight may be gained from the analysis of the components of $\underline{\underline{D}}$ obtained from the 3D-PIV measurements as discussed later in Sec. 4.2.

All the normalized components of $\underline{\underline{D}}$ are shown in Fig. 6 for each valve type. The cases A1, A2, and A3 involving biological valves are represented by Figs. 6(*a*), 6(*b*) and 6(*c*), respectively. The first two plots show the effect of an increase of 39% in the cardiac output for the same valve type. Not surprisingly, higher outputs imply higher axial strains (around a 50% variation), even though the shapes of the curves change only slightly and the peak value $D_{yz}/\lambda \simeq 2.6$ is attained at $t/T \simeq 0.3$. However, the amplitude of the extensional component is at least half the size of the corresponding amplitudes of the two shear components. Interestingly, at higher cardiac outputs (case A3) the opposite behavior is observed: the extensional component, D_{zz}, is twice as large as the shear components D_{xz} and D_{yz} and reaches a peak value of approximately 2.2. The ratio between components remains the same nonetheless.

The plots in the last two figures correspond to the mechanical prostheses. Figure 6(*d*) shows how components other than the

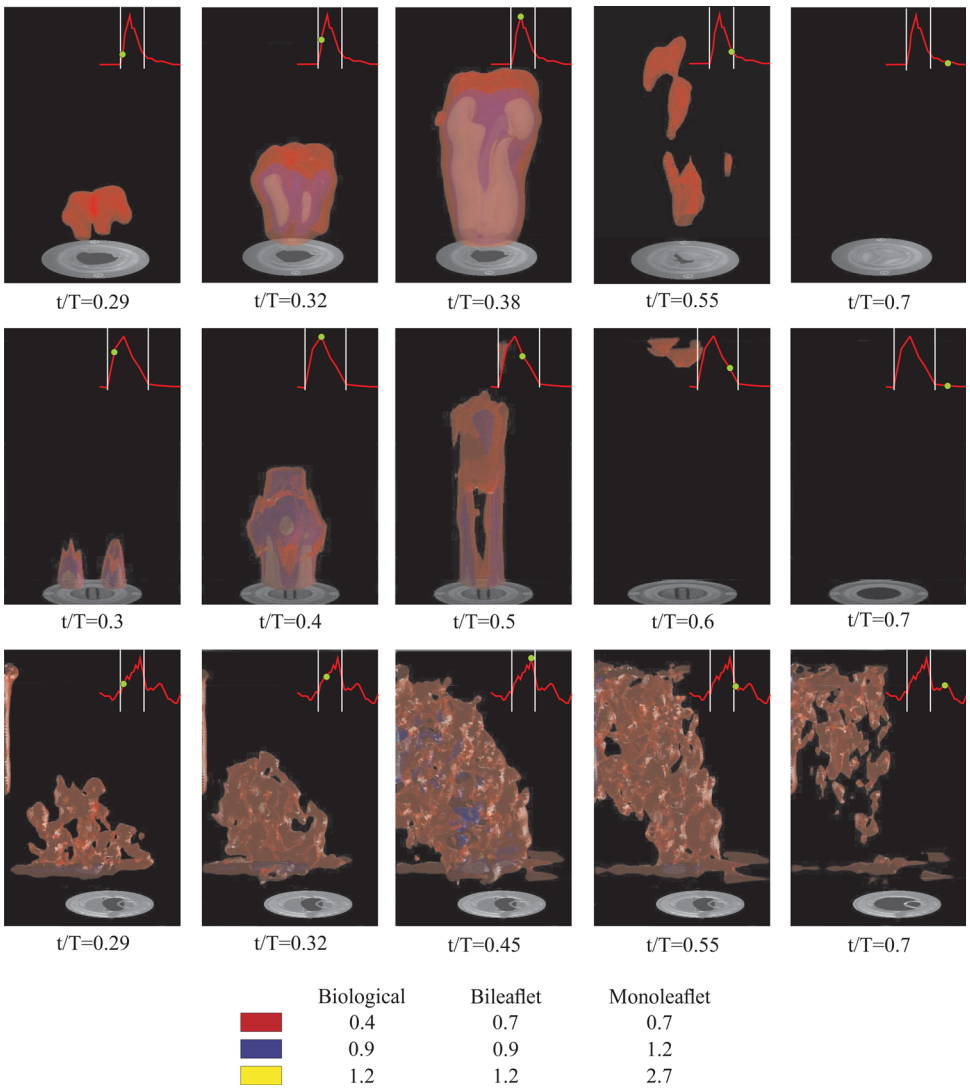

Fig. 5 Shear strain field produced by the selected valves. The first, second and third rows correspond to the biological *A*3, the bileaflet and the monoleaflet, respectively. The images in any given row represent a time sequence for the valve within one period, *T*, of the operating cycle. The highest normalized shears are shown in yellow and the lowest in red according to the color scale at the bottom (specific to each valve type). Additionally, an insert at the upper right corner of each image shows the peak velocity, $|v|_{max}$, measured at that particular instant of the cardiac cycle [actual values can be read from Fig. 3(*a*)]. A photo of the valve at the particular flow condition appear at the bottom of each image.

axial ones are affected by the presence of the bileaflet obturator. In particular, components oriented in transverse directions (e.g., D_{xx} or D_{xy}) become almost as meaningful as the axial components. Moreover, peak values between 1.5 and 2 are attained by all the components of $\underline{\underline{D}}$ at different times during a major part of the cycle ($\Delta t \approx 0.6\,T$). This is clear evidence of a broader disarrangement of the flow field, whence the direction of the flow ceases to be so dominant. As a result, a blood cell element laying in this region would be deformed, twisted and stretched more often along directions other that do not necessarily coincide with the flow direction.

The extreme situation is observed with the Björk-Shiley monoleaflet valve [Fig. 6(*e*)]. Very high strain fluctuations are clearly seen in all directions with several peaks occurring at different instants. These fluctuations are produced throughout the whole cardiac cycle, thereby indicating the existence of turbulentlike eddies. The influence of leakage jets is also significant toward the end and the beginning of the cycle.

It must be remarked that transversal components of the strain tensor are now as important as the axial components. For instance, the peak value of the axial extension is $D_{zz}/\lambda \simeq 4.8$ (almost twice as much as in all other cases) while $D_{xy}/\lambda \simeq 4$. Hence, since a clear distinction between elongation and shear deformation is no longer possible, a blood component in this region would be frequently compressed, stretched and twisted, randomly throughout the entire cardiac cycle. Furthermore, according to Fig. 5, these fluctuations are conveyed far downstream of the valve and could be associated to the cumulative trauma of such blood constituents.

3.4 Straining Frequency Distributions. To help understand how frequently would the blood constituents be subjected to intense strains during the operation of the valve, the average number of times that a particular value of $|\underline{\underline{D}}|$ was registered in the measuring plane at a given instant, t/T, was counted. These results are presented in the form of histograms in Fig. 7.

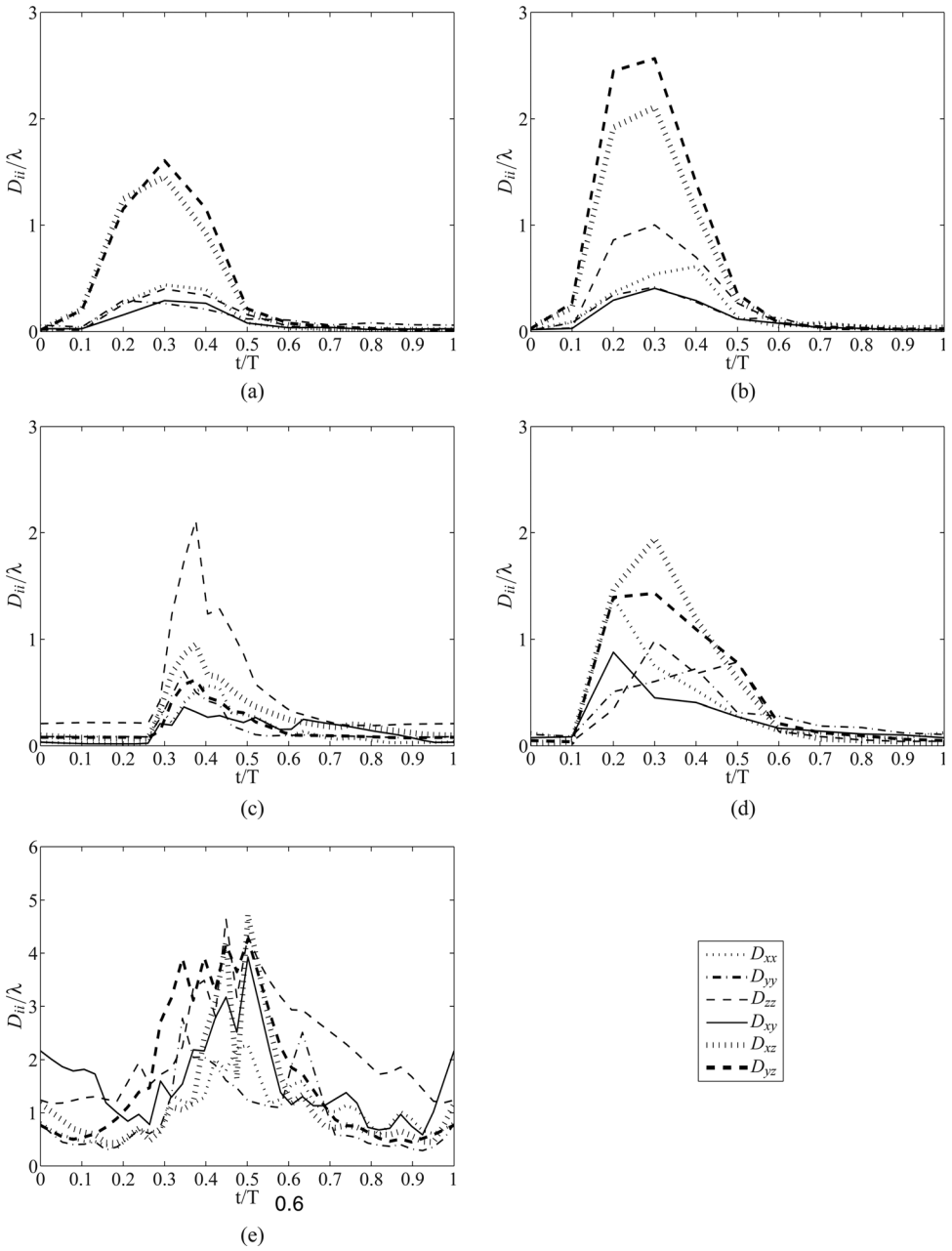

Fig. 6 Components of the strain tensor measured 10 mm downstream of the tested valves. The ranges shown in figures (*a*) Biological A1, (*b*) Biological A2, (*c*) Biological A3, and (*d*) Bileaflet, is $0 \le D_{ii}/\lambda \le 3$. (*e*) In the corresponding range, Monoleaflet is $0 \le D_{ii}/\lambda \le 6$. It is also noted that the main flow is oriented in the z-direction.

Figure 7(*a*) shows the occurrence frequency of the shear magnitude for the biological prosthesis with an increased cardiac output (case A2). It is observed that low magnitude values are evenly distributed along the cardiac cycle with a relatively low number of occurrences ($f \le 5$). The highest shears ($|\underline{\underline{D}}|/\lambda \simeq 2$) are significantly less frequent at $t/T \approx 0.3$ with $f \le 1.5$, and are constrained to a narrow time band of $\Delta t \approx 0.1\,T$. This implies a small likelihood of having a blood component repeatedly acted upon by elevated shear stresses.

For the case of the bileaflet artificial valve (St. Jude Medical) the frequency distribution is shown in Fig. 7(*b*). Here the situation is somewhat different because low and intermediate shears occur much more repeatedly in the interval $0.2 < t/T < 0.3$. However, the number of events drops substantially for higher values. As a matter of fact, shear with normalized values above 2 occur less than 5 times in the measuring plane at $t/T \approx 0.3$, while the highest shearing peaks rarely take place. It is also pointed out that the overall duration of the straining process is quite short and has no effect, whatsoever, for nearly one half of the cycle. On this basis, it can be surmised that a blood element would be subjected to elevated stresses more often than in the case of a biological valve, but the damaging potential would only be moderately increased due to the short duration of the process.

In contrast, the characteristic frequency distribution of the monoleaflet prosthesis (Björk Shiley) reveals another undesired feature of this valve type. In this case, very high strains ($|\underline{\underline{D}}|/\lambda > 3$) are observed to occur at various instants with $f \sim 2$, because the irregular nature of the flow favors a substantial

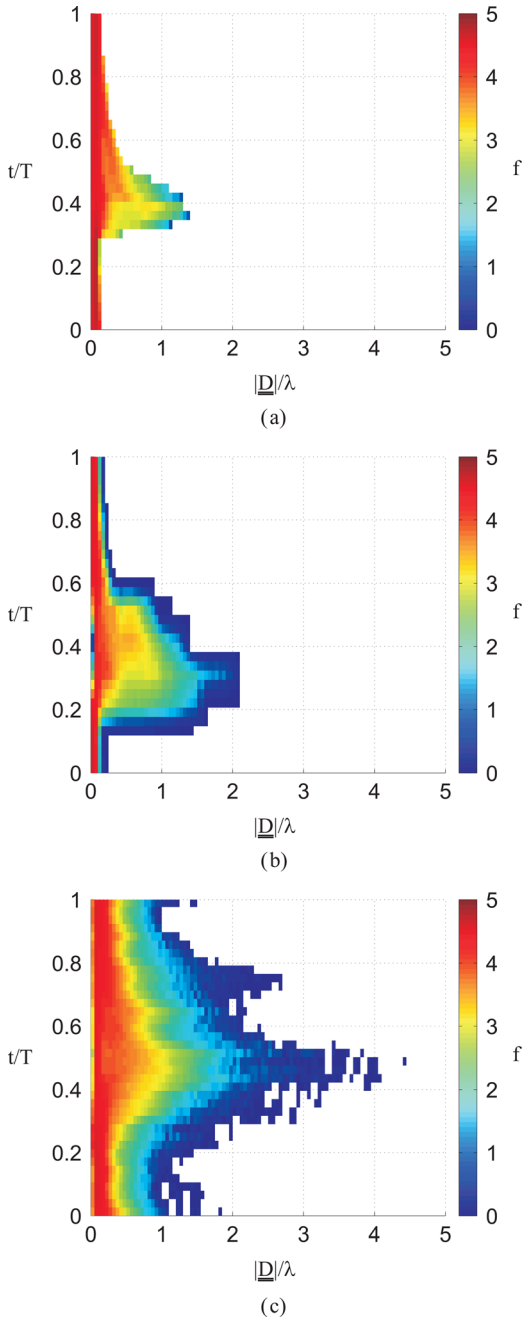

Fig. 7 Frequency histograms for the Biological A2 (*a*), the Bileaflet (*b*), and the Monoleaflet (*c*) prostheses. The frequency *f* represents the number of times that a value of $|\underline{\underline{D}}|/\lambda < 2$ occurs on the measuring plane at time *t/T*. The color scale spans the full frequency range, with red indicating the highest values in each case.

spreading of the smaller eddies. As a result, any blood element would be subjected to abrupt shear variations at a given point. Then, as this element proceeds from one location to another, it would have to endure the process many more times due to the wider spatial extension of the fluctuating field (cf. Sec. 3.2). Furthermore, since these magnitude and frequency levels are present for a larger portion of the cardiac cycle, a greater number of cells, platelets and blood constituents would be affected. These considerations suggest that all such contributions are directly related to the cumulative blood trauma history. Under these circumstances the damage potential of the monoleaflet design is found to be superior to the damage potential of the other models.

4 Discussion

4.1 Rheological Aspects of Blood Flow Through Large Vessels. Some issues concerning the behavior of blood in stress fields are now considered. First, it is important to emphasize that the rheological response of the blood is mainly influenced by the prevailing stress conditions and the size of the vessel where it is flowing. More concretely, blood viscosity has been shown to be highly dependent on the formation of red blood cell aggregations (the so-called "RBC rouleaux aggregates") which are in turn enhanced, or inhibited, by the transient shearing produced in the flow field of small vessels (e.g., Refs. [30,31]). RBC's aggregates would be formed at rather low stress levels (10^1–10^2 mPa) and would have the effect of reducing the apparent viscosity in order to facilitate the flow of blood from the capillary to the venous system. In contrast, at moderate-to-high stresses the formation of rouleaux is inhibited and the viscosity in large vessels is primarily due to the viscosity of the plasma (which behaves as a Newtonian fluid). In view of these considerations and the fluctuating character of the stresses associated with the strain fields presented in this study, it could be concluded that even at short length scales (e.g., those related to small eddies) the apparent viscosity would not be substantially modified. It could also be expected that the activation and damaging processes of the blood constituents would be initiated by stresses beyond the aggregates' inhibition threshold level. Possible interactions and collisions taking place among the various blood elements would be more likely above this threshold, as well. It is worth mentioning that the multiphase nature of the blood must not be ignored because it could promote other important effects at the microscopic level. Therefore, a direct extrapolation of the reported values could result in an underestimation of the actual deformations undergone by elements such as the erythrocytes.

4.2 Relevance of the Extensional Components. According to most authors (e.g., Refs. [4–6,8]) blood damage would be expected to increase in the high strain regions identified in Sec. 3.2. However, a description based exclusively on maximum values could be insufficient to adequately assess the damaging potential of a given prosthesis. For instance, other recent studies (see for example Refs. [19,32]) also suggest that elongation plays a fundamental role in the deformation of membranes and capsules (such as those of blood cells) immersed in flows. Therefore, considering the relative importance of all the strain tensor components is a necessity for this kind of analysis. As evidenced by the results presented in Sec. 3.3 the elongational effects are as important as the purely shearing effects throughout the entire cardiac cycle. It has also been observed how the elongational components stretch (or compress) a given blood element, while the shearing components would not have significant effects at that particular moment. Within this context it is remarked that these considerations must be made for each particular case. For instance, a blood element (e.g., red blood cell, von Willebrand factor) in the flow field produced by a bioprosthesis could be elongated more than it would be deformed in a shear-wise manner depending on the cardiac output [see Fig. 6(*c*)].

If in addition the spatial and temporal variations of each strain component are considered, an improved description of the blood damaging potential could be obtained. In order to complement and relate the damaging potential with the blood trauma history, the exposure and residence times which are known to be key factors in the platelet and von Willebrand factor activation processes (e.g., Refs. [3,5,7]) should also be taken into account.

One final remark should be made concerning the strains in the fluid. Since the strain tensor components have been described in terms of a cartesian frame of reference situated at the valve and oriented in the direction of the flow, the scalar quantity $|\underline{\underline{D}}|$ [cf. Eq. (3)] is used as a measure of the "magnitude" of the strains instead of the usual tensor invariants, which indicate deformation states along the principal directions.

5 Conclusions

The experimental results obtained in this investigation complement the results of other authors who have previously surveyed the basic structure of the flow field produced by prosthetic heart valves. A series of experiments were conducted to compare four typical artificial heart valves: two biological and two mechanical types (bileaflet and monoleaflet). Stereoscopic PIV measurements allowed the identification of the velocity fields in each case and, consequently, all the components of the strain tensor.

Velocities, shear magnitudes and pressure drops were plotted for each model in order to identify the basic characteristics of a satisfactorily performing valve. The velocity field was fully visualized to show the detailed spatial extension and the temporal evolution of the corresponding flow structures.

One of the main objectives of the study was to determine the relative magnitude of the components of the shear tensor throughout the cycle. The importance of this analysis stems from the fact that most investigations concerning blood damage involve only pure shearing conditions. Nonetheless, other studies indicate that the extensional effects are also relevant in the membrane deformation process of the capsules and droplets (see for instance Refs. [19,32]). In the present study it was found that the extensional components of the strain tensor are as significant as the shear components, and that their magnitudes become increasingly important in more agitated flow fields (like the ones produced by the monoleaflet valve type, for example).

The analysis of the strain components, together with the frequency histograms for the variations of corresponding magnitudes, allows a more general description of the blood damaging potential of each prosthesis. In particular, a connection is attempted with the cumulative trauma history of the blood constituents.

In agreement with previous observations, it was found that biological valves produce a regular velocity field and a compact, low-strength, shearing core that developers for only a reduced fraction of the cardiac cycle. Thus, regarding the biological prosthesis as a suitable benchmark, it is concluded that future designs should tend to produce single central jets (with peak velocities in the range 6 m/s to 7 m/s) and single compact shear cores with $|\underline{\underline{D}}|/\lambda < 2$. The development of the ensuing flow should not induce secondary eddies downstream of the valve. Moreover, designs with lower damaging potentials would be characterized by having an approximate ratio of 2:1 between the elongational and the shear components in the axial direction. Other components would also have to remain below this level.

Acknowledgment

The authors wish to thank the financial support of CONACYT-México (Grant No. 102527) to conduct this investigation.

Nomenclature

$\underline{\underline{D}}$ = strain tensor
d_0 = aperture diameter
L = velocity gradient
P = pressure
T = cycle period
t = time
v = velocity
x = position coordinate

Greek Symbols

λ = characteristic frequency
ρ = density
τ = shear stress

Subscripts

i, j = Rectangular components
max = maximum value

Superscripts

* = dimensionless quantity

References

[1] Yoganathan, A., He, Z., and Jones, S., 2004, "Fluid Mechanics of Heart Valves," Annu. Rev. Biomed. Eng., **6**, pp. 331–362.
[2] Einav, S., and Bluestein, D., 2004, "Dynamics of Blood Flow and Platelets Transport in Pathological Vessels," Ann. N.Y. Acad. Sci., **1015**, pp. 351–366.
[3] Sallam, A. M., and Hwang, N. H. C., 1984, "Human Red Blood Hemolysis in a Trubulent Shear Flow: Contribution of Reynolds Shear Stresses," Biorheology, **21**, pp. 783–797.
[4] Giersiepen, M., Wurzinger, L. J., Opitz, R., and Reul, H., 1990, "Estimation of Shear Stress-Related Blood Damage in Heart Valve Protheses -In Vitro Comparison of 25 Aortic Valves," Int. J. Artif. Organs, **13**(5), pp. 300–306.
[5] Kroll, M., Hellums, J., Mclntire, L., Schafer, A., and Moake, J., 1996, "Platelets and Shear Stress," J. Am. Soc. Hematol., **88**(5), pp. 1525–1541.
[6] Hellums, D., 1994, "1993 Whitaker Lecture: Biorheology in Thrombosis Research," Ann. Biomed. Eng., **22**, pp. 445–455.
[7] Schneider, S., Nuschele, S., Wixforth, A., Gorzelanny, C., Alexander-Katz, A., Netz, R., and Schneider, M., 2007, "Shear-Induced Unfolding Triggers Adhesion of von Willebrand Factor Fibers," Proc. Natl. Acad. Sci. U.S.A., **104**(19), pp. 7899–7903.
[8] Bluestein, D., Yin, W., Perrota, P., and Jetsy, J., 2004, "Flow-Induced Platelete Activation in MHV," J. Heart Valve Dis, **13**(3), pp. 501–508.
[9] Yin, W., Alemu, Y., Affeld, K., Jesty, J., and Bluestien, D., 2004, "Flow-Induced Platelet Activation in Bileaflet and Monoleaflet Mechanical Heart Valves," Ann. Biomed. Eng., **32**(8), pp. 1058–1066.
[10] Hanle, D. D., Harrison, E. C., Yoganathan, A. P., Allen, D. T., and Corcoran, W. H., 1989, "In Vitro Flow Dynamics of Four Prosthetic Aortic Valves: A Comparative Analysis," J. Biomech., **22**(6), pp. 597–607.
[11] Chandran, K. B., Khalighi, B., and Chen, C. J., 1985, "Experimental Study of Physiological Pulsatile Flow Past Valve Protheses in a Model of Human Aorta—II. Tilting Disc Valves and the Effect of Orientation," J. Biomech., **18**(10), pp. 773–780.
[12] Zimmer, R., Steegers, A., Paul, R., Affeld, K., and Reul, H., 2000, "Velocities, Shear Stresses and Blood Damage Potential of the Leakage Jets of the Meditronic Parallel Bileaflet Valve," Int. J. Artif. Organs, **23**(1), pp. 41–48.
[13] Manning, K. B., Kini, V., Fontaine, A. A., Deutsch, S., and Tarbell, J. M., 2003, "Regurgitant Flow Field Characteristics of the St. Jude Bileaflet Mechanical Heart Valve Under Physiologic Pulsatile Flow Using Particle Image Velocimetry," Artif. Organs, **27**(9), pp. 840–846.
[14] Kaminsky, R., Kallweit, S., Weber, H. J., Claessens, T., Jozwik, K., and Verdnock, P., 2007, "Flow Visualization Through Two Types of Aortic Prosthetic Hear Valves Using Stereoscopic High-Speed Particle Image Velocitmetry," Artif. Organs, **31**(12), pp. 869–879.
[15] Lim, W. L., Chew, Y. T., Chew, T. C., and Low, H. T., 1997, "Steady Flow Velocity Field and Turbulent Stress Mappings Downstream of a Porcine Bioprosthetic Aortic Valve In Vitro," Ann. Biomed. Eng., **25**, pp. 86–95.
[16] Lim, W. L., Chew, Y. T., Chew, T. C., and Low, H. T., 2001, "Pulsatile Flow Studies of a Porcine Bioprosthetic Aortic Valve In Vitro: PIV Measurements and Shear-Induced Blood Damage," J. Biomech., **34**, pp. 1417–1427.
[17] Marassi, M., Castellini, P., Pinotti, M., and Scalise, L., 2004, "Cardiac Valve Prothesis Flow Performance Measured by 2D and 3D-Stereo Particle Image Velocimetry," Exp. Fluids, **36**, pp. 176–186.
[18] Amatya, D., Troolin, D. R., and Longmire, E. K., 2009, "3D3C Velocity Measurements Downstream of Artificial Heart Valves," 8th International Symposium on Particle Image Velocimetry.
[19] Reyes, M. A., 2005, *Hydrodynamics of Deformable Objects in Creeping Flows*, Ph.D. dissertation, Universidad Nacional Autónoma de México, Mexico City, Mexico.
[20] Grigioni, M., Morbiducci, U., D'Avenio, G., Di Benedetto, G., and Del Gaudio, C., 2005, "A Novel Formulation for Bblood Trauma Prediction by a Modified Power-Law Mathematical Model," Biomech. Model. Mechanobiol., **4**(4), pp. 249–260.
[21] Grigioni, M., Daniele, C., Morbiducci, U., D'Avenio, G., Di Benedetto, G., and Barbaro, V., 2004, "The Power-Law Mathematical Model for Blood Damage Prediction: Analytical Developments and Physical Inconsistencies," Artif. Organs, **28**(5), pp. 467–475.
[22] Gu, L., and Smith, W. A., 2005, "Evaluation of Computational Model for Hemolysis Estimation," ASAIO J., **51**(3), pp. 202–207.
[23] Fung, Y., 1997, *Biomechanics:Circulation*, 2nd ed., Springer, New York.
[24] Diourt, B., Sich, J., Comparat, V., Baguet, J., and Mallion, J., 1999, "Study of Arterial Blood Pressure by a Windkessel-Type Model: Influence of Arterial Functional Properties," Comput. Methods Programs Biomed., **60**, pp. 11–22.
[25] Sequeira, A., and Janela, J., 2007, "An Overview of Some Mathematical Model of Blood Rheology," *A Portrait of State-of-the-Art Research at the Technical University of Lisbon*, Springer, New York, pp. 65–87.

[26] Strackee, J., and Westerhof, N., 1993, *Medical Science Series: The Physics of Heart and Circulation*, 1st ed., Institute of Physics Publishing, Bristol, U.K.
[27] Özcan, O., Meyer, K. E., and Larsen, P. S., 2005, "Measurement of Mean Rotation and Strain-Rate Tensors by Using Stereoscopic PIV," Exp. Fluids, **39**, pp. 771–783.
[28] Holman, J. P., 1994, *Experimental Methods for Engineers*, 6th ed., McGraw-Hill, New York.
[29] Lourenco, L., and Krothapalli, A., 1995, "On the Accuracy of Velocity and Vorticity Measurements With PIV," Exp. Fluids, **18**, pp. 421–428.
[30] Alonso, C., Pries, A. R., and Gaehtgens, P., 1993, "Time-Dependent Rhelogical Behavior of Blood at Low Shear in Narrow Vertical Tubes," Am. J. Physiol. Heart Circ. Physiol., **265**, pp. H553–H561.
[31] Barshtein, G., Wajnblum, D., and Yedgar, S., 2000, "Kinetics of Linear Rouleaux Formation Studied by Visual Monitoring of Red Cell Dynamic Organization," Biophys. J., **78**, pp. 2470–2474.
[32] Barthés-Biesel, D., 2011, "Modelling the Motion of Capsules in Flow," Curr. Opin. Colloid Interface Sci., **16**, pp. 3–12.
[33] Dasi, L., Ge, L., Simon, H., Sotiropoulos, F., and Yoganathan, A., 2007, "Vorticity Dynamics of a Bileaflet Mechanical Heart Valve in an Axisymmetric Aorta," Phys. Fluids, **19**, pp. 1–17.